

# Infrared Spectra of $\text{CH}_3\text{-CrH}$ , $\text{CH}_3\text{-WH}$ , $\text{CH}_2\text{=WH}_2$ , and $\text{CH}\equiv\text{WH}_3$ Formed by Activation of $\text{CH}_4$ with Cr and W Atoms

Han-Gook Cho

Department of Chemistry, University of Incheon, 177 Dohwa-dong, Nam-ku, Incheon, 402-749, South Korea

Lester Andrews\*

Department of Chemistry, University of Virginia, P.O. Box 400319, Charlottesville, Virginia 22904-4319

Colin Marsden

Laboratoire de Physique Quantique, UMR 5626, IRSAMC, Université Paul Sabatier, 118 Route de Narbonne, 31062 Toulouse Cedex 4, France

Received June 30, 2005

Laser-ablated W atoms react with  $\text{CH}_4$  in excess argon to form the  $\text{CH}_3\text{-WH}$ ,  $\text{CH}_2\text{=WH}_2$ , and  $\text{CH}\equiv\text{WH}_3$  molecules with increasing yield in this order of product stability. These molecules are identified from matrix infrared spectra by isotopic substitution. Tungsten methylidene and methylidyne hydride molecules are reversibly interconverted by  $\alpha\text{-H}$  transfers upon visible and ultraviolet irradiations. Matrix infrared spectra and DFT/B3LYP calculations show that  $\text{CH}\equiv\text{WH}_3$  is a stable molecule with  $C_{3v}$  symmetry, but other levels of theory were required to describe agostic distortion for  $\text{CH}_2\text{=WH}_2$ . Analogous reactions with Cr gave only  $\text{CH}_3\text{-CrH}$ , which is calculated to be by far the most stable product.

## Introduction

The Group 4 transition metals activate methane to give the simple methylidene dihydrides,  $\text{CH}_2\text{=MH}_2$ , which exhibit  $\text{CH}_2$  distortion owing to an agostic interaction.<sup>1–3</sup> Calculations using large basis sets show that the two metal hydride bond lengths are different and that the  $\text{CH}_2$  subunit is distorted with  $\text{H-C-M}$  angles of 91.6, 92.9, and 95.6° for  $\text{M} = \text{Ti}$ ,  $\text{Zr}$ , and  $\text{Hf}$ , respectively.<sup>4–7</sup> The analogous methylidene complexes prepared from methyl fluoride, namely  $\text{CH}_2\text{=MHF}$ , showed the same trend in agostic bonding.<sup>8–10</sup>

Organometallic chemistry has many examples of high-oxidation-state transition metal alkylidene complexes ( $\text{R}_1\text{R}_2\text{-C=M}$ ) where bulky substituents are required to stabilize the electron-deficient metal center, and many of these compounds are agostic.<sup>11</sup> These complexes play important roles in synthetic chemistry for alkane activation and alkene metathesis reactions.<sup>11–13</sup> In addition, the alkylidene complexes of Group 6 can rearrange into the analogous alkylidyne complexes ( $\text{RC}\equiv\text{M}$ ), and a number of  $\text{RC}\equiv\text{MX}_1\text{X}_2\text{X}_3$  complexes have been prepared.<sup>12</sup> Recently, we investigated Mo atom reactions with methane to explore further agostic bonding in simple  $\text{CH}_2\text{=MH}_2$  methylidene complexes, and we find the agostic distortion to be less ( $\text{H-C-Mo}$  angle = 113.0°) for  $\text{CH}_2\text{=MoH}_2$ .<sup>14</sup> In addition, visible photolysis

\* To whom correspondence should be addressed. E-mail: isa@virginia.edu.

- (1) Scherer, W.; McGrady, G. S. *Angew. Chem., Int. Ed.* **2004**, *43*, 1782.
- (2) Clot, E.; Eisenstein, O. Agostic Interactions from a Computational Perspective. In *Structure and Bonding, Computational Inorganic Chemistry*; Kaltzoyannis, N., McGrady, J. E., Eds.; Springer-Verlag: Heidelberg, 2004; pp 1–36.
- (3) Ujaque, G.; Cooper, A. C.; Maseras, F.; Eisenstein, O.; Caulton, K. G. *J. Am. Chem. Soc.* **1998**, *120*, 361.
- (4) Andrews, L.; Cho, H.-G.; Wang, X. *Angew. Chem.* **2005**, *117*, 115.
- (5) Cho, H.-G.; Wang, X.; Andrews, L. *J. Am. Chem. Soc.* **2005**, *127*, 465.
- (6) Andrews, L.; Cho, H.-G.; Wang, X. *Inorg. Chem.* **2005**, *44*, 4834.
- (7) Cho, H.-G.; Wang, X.; Andrews, L. *Organometallics* **2005**, *24*, 2854.

- (8) Cho, H.-G.; Andrews, L. *J. Phys. Chem. A* **2004**, *108*, 6294.
- (9) Cho, H.-G.; Andrews, L. *J. Am. Chem. Soc.* **2004**, *126*, 10485.
- (10) Cho, H.-G.; Andrews, L. *Organometallics* **2004**, *23*, 4357.
- (11) Schrock, R. R. *Chem. Rev.* **2002**, *102*, 145.
- (12) Buchmeiser, M. R. *Chem. Rev.* **2000**, *100*, 1565.
- (13) Crabtree, R. H. *Chem. Rev.* **1985**, *85*, 245.
- (14) Cho, H.-G.; Andrews, L. *J. Am. Chem. Soc.* **2005**, *127*, 8226.

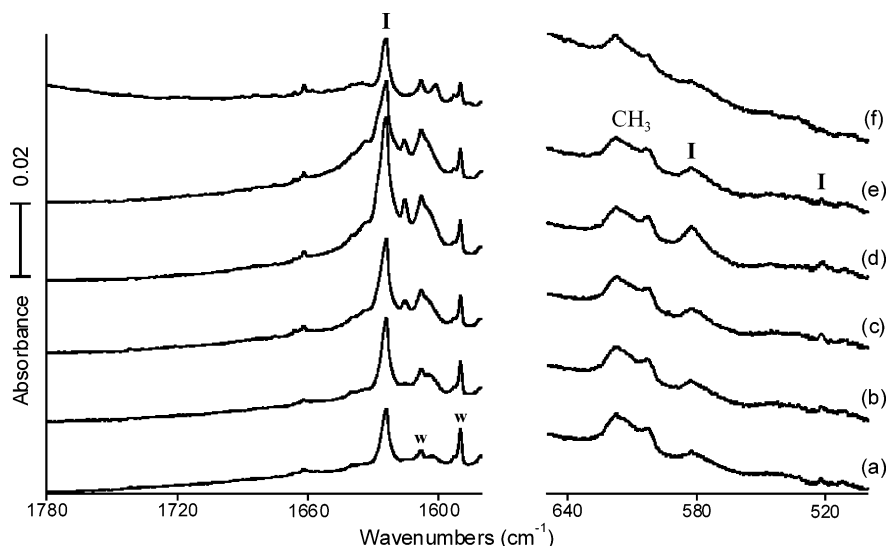


**Figure 1.** Infrared spectra in the 1780–1580 and 640–520  $\text{cm}^{-1}$  regions for the products of laser-ablated Cr atom reactions with  $\text{CH}_4$  in excess argon. (a) 2%  $\text{CH}_4$  and Cr deposited for 60 min, (b)  $\lambda > 420$  nm irradiation for 20 min, (c) after 240–380 nm irradiation, (d) after  $\lambda > 290$  nm irradiation, (e) after  $\lambda > 220$  nm (full-arc) irradiation, and (f) after annealing to 26 K. Water impurity absorptions are marked w.

initiates  $\alpha$ -H transfer to form the simplest methylidyne hydride complex,  $\text{HC}\equiv\text{MoH}_3$ .<sup>14</sup> Similar reactions with Mo and  $\text{CH}_3\text{F}$  have been studied, and the  $\text{CH}_2\text{=MoHF}$  and  $\text{CH=MoH}_2\text{F}$  molecules have been characterized.<sup>15</sup> Since there appear to be more examples of  $\text{RC}\equiv\text{W}$  complexes in the literature,<sup>11</sup> we report here analogous reactions of tungsten with methane, which produce  $\text{CH}_3\text{-WH}$ ,  $\text{CH}_2\text{=WH}_2$ , and the 3-fold-symmetric  $\text{HC}\equiv\text{WH}_3$  molecule, and with chromium, which forms only the most stable  $\text{CH}_3\text{-CrH}$  insertion product.

### Experimental and Computational Methods

The laser-ablation matrix-infrared experiment has been described previously.<sup>16,17</sup> Briefly, laser-ablated chromium and tungsten atoms (Johnson–Matthey) were reacted with  $\text{CH}_4$  (Matheson, UHP grade),  $^{13}\text{CH}_4$ ,  $\text{CD}_4$ , and  $\text{CH}_2\text{D}_2$  (Cambridge Isotopic Laboratories) in excess argon (MG Industries) during condensation on a CsI window at 8 K. Infrared spectra were recorded at 0.5  $\text{cm}^{-1}$  resolution on a Nicolet 550 spectrometer with type B HgCdTe detector. Samples were irradiated by a mercury arc lamp (175 W, globe removed) for 20 min periods, were annealed, and more spectra were recorded.

Supporting electronic structure calculations were done using the Gaussian 98 and 03 packages,<sup>18a</sup> B3LYP density functional,<sup>18b</sup> 6-311++G(2d, p) basis set for H, C, and Cr, 6-311++G(3df, 3pd) basis sets for C, H<sup>18c</sup> and SDD effective core potential and basis set for W (14 valence electrons),<sup>18d</sup> the VSXC density functional,<sup>18e</sup> and the MP2 and CCSD methods with TZ2P and SDD+2f basis sets to provide structures and vibrational frequencies for possible reaction products. Geometries were fully relaxed during optimization, and the optimized geometry was confirmed through vibrational analysis.

### Results

The products of methane activation by Cr and W atoms will be characterized by matrix infrared spectroscopy and electronic structure calculations.

**Infrared Spectra.** Laser-ablated Cr atoms and  $\text{CH}_4$  were mixed in argon, condensing at 8 K, and Figure 1 illustrates infrared spectra of the resulting sample. The strongest new absorption at 1623.9  $\text{cm}^{-1}$  (labeled I) in the water region is just above the strong fundamental for  $\text{CrH}_2$  at 1614.5  $\text{cm}^{-1}$ , which is not observed here.<sup>17</sup> This band increases slightly on visible ( $\lambda > 420$  nm irradiation) and more so on near-ultraviolet (240–380 nm and  $\lambda > 290$  nm) irradiation. Other absorptions at 582.3 and 521.5  $\text{cm}^{-1}$  exhibit the same photolysis behavior. These samples also reveal absorptions common to other methane experiments including  $\text{Ar}_7\text{H}^+$ ,  $\text{CH}_3$  radical,  $\text{C}_2\text{H}_2$ ,  $\text{C}_2\text{H}_4$ , and  $\text{C}_2\text{H}_6$ .<sup>19–24</sup>

Different methane isotopes were also employed. The  $^{13}\text{CH}_4$  reagent produced no shift on the strong 1623.9  $\text{cm}^{-1}$  absorption, but shifted the lower bands to 577.9 and 519.0

(15) (a) Cho, H.-G.; Andrews, L. *Chem. Eur. J.* **2005**, *11*, 5017. (b) Cho, H.-G.; Andrews, L. *Organometallics* **2005**, in press.  
 (16) Andrews, L.; Citra, A. *Chem. Rev.* **2002**, *102*, 885 and references therein.  
 (17) Wang, X.; Andrews, L. *J. Phys. Chem. A* **2003**, *107*, 570.

(18) (a) Frisch, M. J.; Trucks, G. W.; Schlegel, H. B.; Scuseria, G. E.; Robb, M. A.; Cheeseman, J. R.; Montgomery, J. A., Jr.; Vreven, T.; Kudin, K. N.; Burant, J. C.; Millam, J. M.; Iyengar, S. S.; Tomasi, J.; Barone, V.; Mennucci, B.; Cossi, M.; Scalmani, G.; Rega, N.; Petersson, G. A.; Nakatsuji, H.; Hada, M.; Ehara, M.; Toyota, K.; Fukuda, R.; Hasegawa, J.; Ishida, M.; Nakajima, T.; Honda, Y.; Kitao, O.; Nakai, H.; Klene, M.; Li, X.; Knox, J. E.; Hratchian, H. P.; Cross, J. B.; Bakken, V.; Adamo, C.; Jaramillo, J.; Gomperts, R.; Stratmann, R. E.; Yazyev, O.; Austin, A. J.; Cammi, R.; Pomelli, C.; Ochterski, J. W.; Ayala, P. Y.; Morokuma, K.; Voth, G. A.; Salvador, P.; Dannenberg, J. J.; Zakrzewski, V. G.; Dapprich, S.; Daniels, A. D.; Strain, M. C.; Farkas, O.; Malick, D. K.; Rabuck, A. D.; Raghavachari, K.; Foresman, J. B.; Ortiz, J. V.; Cui, Q.; Baboul, A. G.; Clifford, S.; Cioslowski, J.; Stefanov, B. B.; Liu, G.; Liashenko, A.; Piskorz, P.; Komaromi, I.; Martin, R. L.; Fox, D. J.; Keith, T.; Al-Laham, M. A.; Peng, C. Y.; Nanayakkara, A.; Challacombe, M.; Gill, P. M. W.; Johnson, B.; Chen, W.; Wong, M. W.; Gonzalez, C.; Pople, J. A. *Gaussian 03*, revision B.04; Gaussian, Inc.: Wallingford, CT, 2004.  
 (b) Stevens, P. J.; Devlin, F. J.; Chabrowski, C. F.; Frisch, M. J. *J. Phys. Chem.* **1994**, *98*, 11623. (c) Krishnan, R.; Binkley, J. S.; Seeger, R.; Pople, J. A. *J. Chem. Phys.* **1980**, *72*, 650. Frisch, M. J.; Pople, J. A.; Binkley, J. S. *J. Chem. Phys.* **1984**, *80*, 3265. (d) Andrae, D.; Haussermann, U.; Daly, M.; Stoll, H.; Preuss, H. *Theor. Chim. Acta* **1990**, *88*, 123. (e) Van Voorhis, T.; Scuseria, G. E. *J. Chem. Phys.* **1998**, *109*, 400.  
 (19) Jacox, M. E. *J. Mol. Spectrosc.* **1977**, *66*, 272.  
 (20) Milligan, D. E.; Jacox, M. E. *J. Mol. Spectrosc.* **1973**, *46*, 460.  
 (21) Wight, C. A.; Ault, B. S.; Andrews, L. *J. Chem. Phys.* **1976**, *65*, 1244.  
 (22) Wang, X.; Andrews, L. *J. Phys. Chem. A* **2003**, *107*, 337.  
 (23) Cho, H.-G.; Andrews, L. *J. Phys. Chem. A* **2004**, *108*, 3965.  
 (24) Davis, S. R.; Andrews, L. *J. Am. Chem. Soc.* **1987**, *109*, 4768.

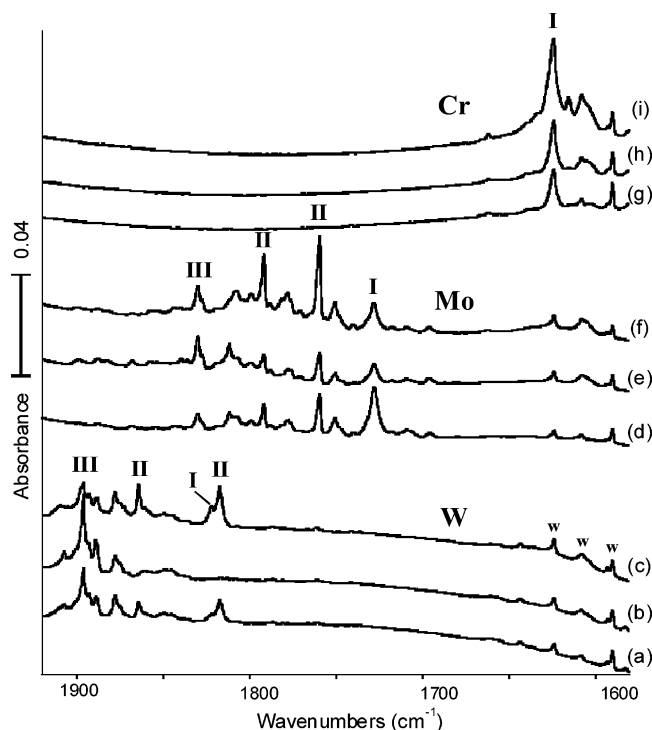


**Figure 2.** Infrared spectra in the 1920–1580  $\text{cm}^{-1}$  region for the products of laser-ablated Group 6 atom reactions with  $\text{CH}_4$  in excess argon. (a) 2%  $\text{CH}_4$  and W deposited for 60 min, (b)  $\lambda > 530$  nm irradiation, (c) after 240–380 nm irradiation, (d) 2%  $\text{CH}_4$  and Mo deposited for 60 min, (e)  $\lambda > 420$  nm irradiation for 20 min, (f) after 240–380 nm irradiation, (g) 2%  $\text{CH}_4$  and Cr deposited for 60 min, (h)  $\lambda > 420$  nm irradiation for 20 min, and (i) after  $\lambda > 290$  nm irradiation. Water impurity absorptions are marked w.

$\text{cm}^{-1}$ . Using  $\text{CD}_4$  shifted the strong band to 1172.3  $\text{cm}^{-1}$  and the stronger lower band to 476.1  $\text{cm}^{-1}$ . The mixed-isotopic  $\text{CH}_2\text{D}_2$  precursor gave strong bands at 1623.9 and 1172.4  $\text{cm}^{-1}$ .

Excited Mo atoms were reacted with  $\text{CH}_4$ , and the details have been reported previously.<sup>14</sup> Major product absorptions were observed at 1728.0, 1759.6, 1791.6, and 1830.0  $\text{cm}^{-1}$

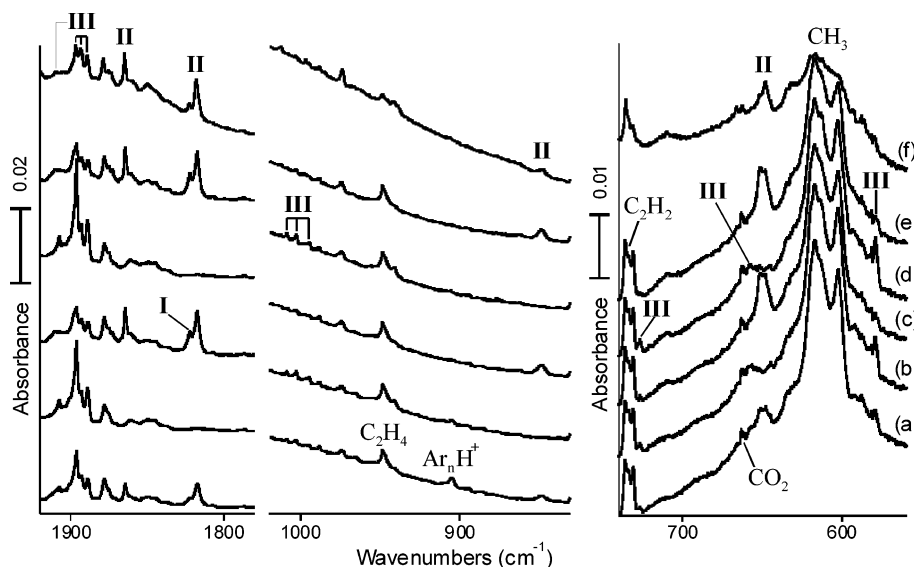


**Figure 3.** Infrared spectra in the 1920–1780 and 1020–930, and 740–560  $\text{cm}^{-1}$  regions for the products of laser-ablated W atom reactions with  $\text{CH}_4$  in excess argon. (a) 2%  $\text{CH}_4$  and W deposited for 60 min, (b)  $\lambda > 530$  nm irradiation, (c) after 240–380 nm irradiation, (d)  $\lambda > 530$  nm irradiation, (e) after 240–380 nm irradiation, and (f) after annealing to 26 K.

in the Mo–H stretching region. These bands are labeled I, II, and III, respectively, in Figure 2, where the infrared spectra of laser-ablated Cr, Mo, and W reaction products with 2%  $\text{CH}_4$  in argon are compared. Additional spectra for visible and near-ultraviolet irradiation are shown for each metal. In the cases of Mo and W, reversible photochemical interconversion among the major products is observed.

Laser-ablated W atoms and  $\text{CH}_4$  were reacted with methane in three experiments, and spectra from the most-productive 2%  $\text{CH}_4$  experiment are shown in Figures 2 and 3. The upper region reveals strong new absorptions at 1817.3 and 1864.5  $\text{cm}^{-1}$  (marked II) and at 1896.3  $\text{cm}^{-1}$  (noted III). Irradiation in the upper visible region ( $\lambda > 530$  nm) virtually destroyed the bands marked II and nearly doubled the bands noted III with a 1907.5  $\text{cm}^{-1}$  sideband. A following near-ultraviolet (240–380 nm) irradiation reduced the III band and restored the II bands to even greater intensity than those formed on sample deposition. In addition, a weak 1822.2  $\text{cm}^{-1}$  absorption, labeled I, increases more on UV irradiation than the II bands. This irradiation cycle was repeated with identical results. The unidentified 1878.0  $\text{cm}^{-1}$  band is not affected by irradiation, and it appears in the W and  $\text{H}_2$  reaction system; however, none of the new product bands are formed in the W +  $\text{H}_2$  experiments.<sup>25</sup> Other bands at lower frequencies follow the II or the III bands on the cycles of wavelength-selective irradiation and thus can be associated with product species II and III, respectively. The product absorption wavenumbers are collected in Table 1.

Again, the  $^{13}\text{CH}_4$  precursor gave no shift in the upper product bands but displaced the lower product absorptions (Table 1). The  $\text{CD}_4$  reagent shifted all product bands, and the upper region is shown in Figure 4. Unfortunately, the II band at 1303.1  $\text{cm}^{-1}$  is close to the  $\text{CH}_4$  impurity absorption, but it and its II partner at 1336.2  $\text{cm}^{-1}$  alternate with the III band set at 1362.8  $\text{cm}^{-1}$  on the visible and near-ultraviolet irradiation cycles.

**Table 1.** Infrared Absorptions (cm<sup>-1</sup>) Observed for Laser-Ablated W Atom and Methane Reaction Products in Excess Argon

CH <sub>4</sub>	<sup>13</sup> CH <sub>4</sub>	CD <sub>4</sub>	CH <sub>2</sub> D <sub>2</sub>	identity <sup>a</sup>
1907.5	1907.5	—	1903.4, 1899.3	III
1896.3	1986.2	1362.8	1895.6, 1363.1	III
1893.1	1893.0	—	—	III
1888.3	1888.2	1355.5	1888.8, 1356.0	III
1878.0	1878	1347	—	WH <sub>x</sub>
1864.5	1864.4	1336.2	1864.8, 1863.1, 1336.9, 1820.3,	II
—	—	—	—	II
1822.2	1822.0	—	—	I
1817.2	1817.2	1303.1	1818.2, 1816.2	II
1008.9	975.5	—	—	III
1003.4	970.7	953.3	—	III
995.1	964.6	—	—	III
904.2	904.2	643.8	904.2, 634.8	Ar <sub>n</sub> H <sup>+</sup> , Ar <sub>n</sub> D <sup>+</sup>
847.8	843.0	712.2	—	II
726.7	719.9	570.5	—	III
658.0	—	(468)	—	III
651.5	646.9	506.2	—	II
617, 603	612, 598	453	—	CH <sub>3</sub> , CD <sub>3</sub>
581.9	582	—	—	III
579.4	579	—	—	III

<sup>a</sup> I denotes CH<sub>3</sub>-WH, II indicates CH<sub>2</sub>=WH<sub>2</sub>, and III identifies CH≡WH<sub>3</sub>.

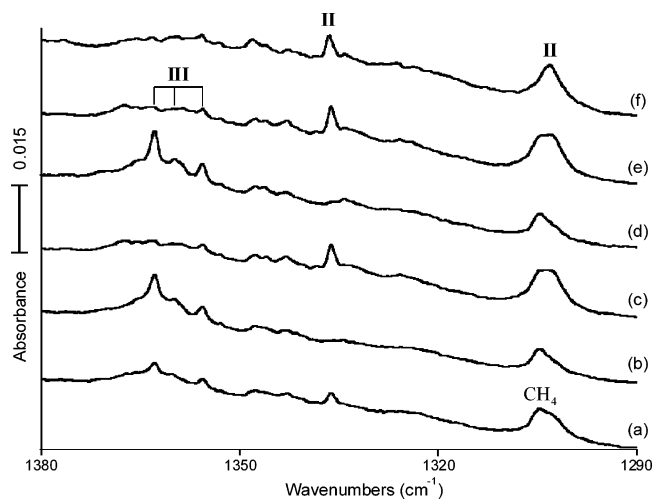


**Figure 4.** Infrared spectra in the 1380–1290 cm<sup>-1</sup> region for the products of laser-ablated W atom reactions with CD<sub>4</sub> in excess argon. (a) 2% CD<sub>4</sub> and W deposited for 60 min, (b) λ > 530 nm irradiation, (c) after 240–380 nm irradiation, (d) λ > 530 nm irradiation, (e) after 240–380 nm irradiation, and (f) after annealing to 26 K.

The CH<sub>2</sub>D<sub>2</sub> precursor provided major II and III bands slightly shifted from values observed for CH<sub>4</sub> and CD<sub>4</sub> and, in addition, new mixed isotopic absorptions marked with arrows at 1903.4 and 1899.3 cm<sup>-1</sup> beside the III bands and at 1849.8 cm<sup>-1</sup> between the II bands in the W–H stretching region in Figure 5. New bands in the W–D stretching region are listed in Table 1.

**Calculations.** Density functional B3LYP calculations were done for CH<sub>3</sub>-CrH, CH<sub>2</sub>=CrH<sub>2</sub>, and CH≡CrH<sub>3</sub> in the quintet, triplet, and singlet ground states found for the analogous molybdenum species,<sup>14</sup> and the structures are illustrated in Figure 6. We were unable to converge CH≡CrH<sub>3</sub> in C<sub>3v</sub> symmetry, and the minimum-energy structure exhibited bonding between two hydrogen atoms on the Cr center, which is reminiscent of CrH<sub>2</sub>-dihydrogen complexes.<sup>17</sup> The CH<sub>2</sub>=CrH<sub>2</sub> structure showed a small

**Table 2.** Harmonic Vibrational Frequencies Calculated for CH<sub>3</sub>-CrH in the Ground Quintet State<sup>a</sup>

CH <sub>3</sub> -CrH	<sup>13</sup> CH <sub>3</sub> -CrH	CD <sub>3</sub> -CrD	mode
3054.0 (14) <sup>b</sup>	3044.4 (14) <sup>b</sup>	2254.2 (5) <sup>b</sup>	A' C–H str
2972.1 (16)	2968.6 (17)	2130.4 (6)	A' C–H str
1674.2 (231)	1674.4 (231)	1196.3 (121)	A' Cr–H str
1439.0 (1)	1435.7 (1)	1045.2 (1)	A' CH <sub>3</sub> scis
1141.8 (5)	1133.1 (6)	891.3 (0)	A' CH <sub>3</sub> deform
603.3 (86)	599.0 (85)	487.7 (55)	A' CH <sub>3</sub> rock
487.9 (11)	477.0 (11)	419.4 (8)	A' C–Cr str
363.3 (76)	363.1 (76)	259.3 (39)	A' CCrH bend
3084.2 (7)	3073.1 (8)	2282.5 (1)	A'' C–H str
1420.8 (2)	1417.5 (2)	1032.3 (3)	A'' CH <sub>3</sub> scis
535.9 (33)	533.3 (33)	400.5 (22)	A'' CH <sub>3</sub> rock
107.6 (72)	107.6 (72)	76.7 (38)	A'' CH <sub>3</sub> tort

<sup>a</sup> All electron 611++G(2d, p) basis. <sup>b</sup> Frequencies, cm<sup>-1</sup> (intensities, km/mol).

amount of distortion. The CH<sub>3</sub>-CrH molecule appears to be similar to CH<sub>3</sub>-MoH,<sup>14</sup> and the computed frequencies are listed in Table 2.

Analogous B3LYP calculations were performed for W this time using the SDD pseudopotential and its associated basis set, and the structures are compared in Figure 6. The structure for quintet CH<sub>3</sub>-WH is similar to those for CH<sub>3</sub>-MoH and CH<sub>3</sub>-CrH as expected, and the strongest infrared absorption is calculated at 1908 cm<sup>-1</sup> (169 km/mol). However, in contrast to the agostic structures calculated for CH<sub>2</sub>=TiH<sub>2</sub>, CH<sub>2</sub>=ZrH<sub>2</sub>, CH<sub>2</sub>=HfH<sub>2</sub>, and CH<sub>2</sub>=MoH<sub>2</sub>,<sup>4–8,14</sup> the structure computed for triplet CH<sub>2</sub>=WH<sub>2</sub> is symmetrical (C<sub>2v</sub>) and does not show any agostic bonding effects. Computed frequencies are listed in Table 3. The first thing to notice is that the WH<sub>2</sub> stretching frequencies are separated by only 14 cm<sup>-1</sup>, a value quite different from the experimental separation of 47 cm<sup>-1</sup>. The SDD+f basis gave slight distortion (H–C–W angles = 121.5°, 122.5°), but the frequencies changed only a few cm<sup>-1</sup>. It appears that B3LYP calculations do not describe ground-state CH<sub>2</sub>=WH<sub>2</sub> correctly. It is interesting to note that a 16 kcal/mol higher energy singlet CH<sub>2</sub>=WH<sub>2</sub> state is highly distorted at carbon. The CH≡WH<sub>3</sub> molecule has C<sub>3v</sub> symmetry, and the calculated frequencies at the B3LYP level are listed in Table 4. The Mulliken charges computed for these species are given in Table S1 (Supporting Information).

To investigate triplet CH<sub>2</sub>=WH<sub>2</sub> in greater detail, calculations were then performed at the MP2, MP4SDQ, and CCSD levels, adopting a TZ2P basis for C and H (d-type exponents on C 1.2 and 0.3, p-type exponents on H 2.0 and 0.5) and the SDD basis for W augmented with two f-type functions (exponents 1.0 and 0.3: the variationally optimum f-type exponent for a single set at the MP2 level is 0.5) The five lowest- and highest-energy MO were frozen for these post-HF calculations. The CH<sub>2</sub>=WH<sub>2</sub> structure displays a strong agostic distortion at all three of these levels of theory, though the details of the distortion vary. The principal geometrical parameters obtained with these post-HF methods are reported in Table 5 together with the main IR-active vibrational wavenumbers. The difference in energy between the C<sub>2v</sub> transition state and the C<sub>s</sub> minimum is also reported. Note also that the VSXC density functional finds a distorted structure. All frequencies computed at the VSXC level are

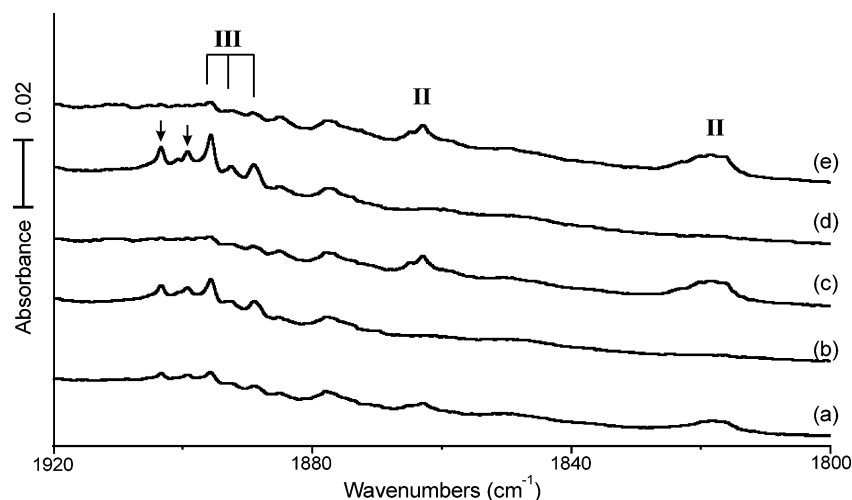


**Figure 5.** Infrared spectra in the 1920–1800  $\text{cm}^{-1}$  region for the products of laser-ablated W atom reactions with  $\text{CH}_2\text{D}_2$  in excess argon. (a) 2%  $\text{CH}_2\text{D}_2$  and W deposited for 60 min, (b)  $\lambda > 530$  nm irradiation, (c) after 240–380 nm irradiation, (d)  $\lambda > 530$  nm irradiation, and (e) after 240–380 nm irradiation.

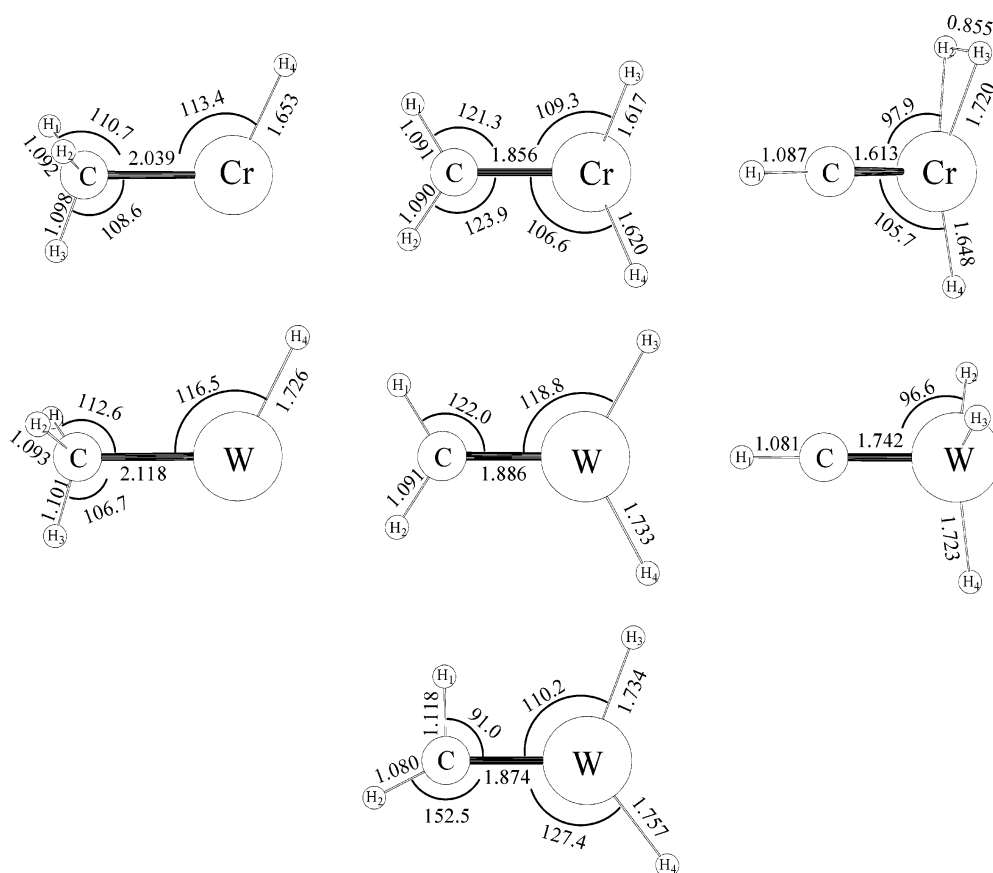


**Figure 6.** Structures computed for  $\text{CH}_3\text{-MH}$  (Q),  $\text{CH}_2\text{=MH}_2$  (T), and  $\text{CH}\equiv\text{MH}_3$  (S) at the B3LYP/6-311++G(3df, 3pd) level of theory: SDD used for W. Single structure calculated for  $\text{CH}_2\text{=WH}_2$  at the CCSD/TZ2P/SDD+2f level. Bond distances, angstroms; bond angles, degrees. Q denotes quintet, T indicates triplet, and S denotes singlet electronic states.

listed in Table S2. The CCSD calculated frequencies are included in Table 3, and the  $\text{CDH}=\text{WHD}$  mixed isotopic molecules are featured in Table 6.

The relative energies computed at the B3LYP level for the Group 6  $\text{CH}_3\text{-MH}$ ,  $\text{CH}_2\text{=MH}_2$ , and  $\text{CH}\equiv\text{MH}_3$  molecules are compared in Figure 7. Notice that the methylidyne trihydride complex is the least stable for Cr but the most stable for W.

Parameters for the simple  $\text{HC}\equiv\text{W}$  alkylidyne molecule were calculated as a calibration since experimental values

are available.<sup>26</sup> For the doublet ground state, we compute 1.082 and 1.732 Å bond lengths and 3223.7 (6 km/mol intensity), 1057.4(12), and 694.6(59)  $\text{cm}^{-1}$  frequencies with B3LYP, which compare favorably with the observed 1.0765, 1.7366 Å and 1006, 660  $\text{cm}^{-1}$  values.

## Discussion

The new product absorptions from Cr and W atom reactions with methane will be identified on the basis of photochemistry, isotopic substitution, and comparison with

**Table 3.** Harmonic Vibrational Frequencies (cm<sup>-1</sup>) Computed for the Triplet Planar Ground State Structure of CH<sub>2</sub>=WH<sub>2</sub>

mode description	<sup>12</sup> CH <sub>2</sub> =WH <sub>2</sub> <sup>a</sup>		<sup>13</sup> CH <sub>2</sub> =WH <sub>2</sub> <sup>a</sup>		CD <sub>2</sub> =WD <sub>2</sub> <sup>a</sup>		<sup>12</sup> CH <sub>2</sub> =WH <sub>2</sub> <sup>d</sup>		<sup>13</sup> CH <sub>2</sub> =WH <sub>2</sub> <sup>d</sup>		CD <sub>2</sub> =WD <sub>2</sub> <sup>d</sup>	
	freq. <sup>b</sup>	int. <sup>c</sup>	freq. <sup>b</sup>	int. <sup>c</sup>	freq. <sup>b</sup>	int. <sup>c</sup>	freq. <sup>b</sup>	int. <sup>c</sup>	freq. <sup>b</sup>	int. <sup>c</sup>	freq. <sup>b</sup>	int. <sup>c</sup>
CH <sub>2</sub> str	3152	(0)	3139		2341	(0)	3238.0	(1)	3226.8		2398.7	(1)
CH <sub>2</sub> str	3053	(2)	3047		2214	(3)	2859.3	(4)	2852.8		2080.3	(4)
WH <sub>2</sub> str	1922	(156)	1922		1361	(79)	1929.3	(177)	1929.3		1368.3	(92)
WH <sub>2</sub> str	1908	(244)	1908		1356	(123)	1887.5	(313)	1887.5		1339.4	(157)
CH <sub>2</sub> scis	1308	(5)	1297		1042	(13)	1363.0	(17)	1353.4		1067.8	(10)
WH <sub>2</sub> bend	891	(23)	889		678	(18)	851.2	(55)	845.8		703.1	(26)
C=W str	736	(11)	717		598	(0)	778.4	(1)	763.8		589.7	(10)
CH <sub>2</sub> rock	700	(3)	695		546	(60)	676.9	(96)	671.8		525.4	(63)
CH <sub>2</sub> wag	698	(89)	692		538	(2)	651.3	(12)	644.6		502.5	(7)
WH <sub>2</sub> wag	524	(0)	524		370	(34)	554.8	(0)	554.6		394.7	(0)
WH <sub>2</sub> rock	246	(67)	246		178	(34)	299.1	(13)	298.7		214.1	(6)
CH <sub>2</sub> twist	97	(0)	97		71	(0)	252.4	(74)	252.1		181.6	(37)

<sup>a</sup> B3LYP/6-311++G(3df, 3pd)/SDD. <sup>b</sup> Frequencies, cm<sup>-1</sup>. <sup>c</sup> Intensities, km/mol. <sup>d</sup> CCSD/TZ2P/SDD+2f.

**Table 4.** Harmonic Vibrational Frequencies Computed<sup>a</sup> for the <sup>1</sup>A<sub>1</sub> Ground State C<sub>3v</sub> Structure of CH≡WH<sub>3</sub>

mode description	<sup>12</sup> CH≡WH <sub>3</sub>		<sup>13</sup> CH≡WH <sub>3</sub>		CD≡WD <sub>3</sub>	
	freq. <sup>b</sup>	int. <sup>c</sup>	freq. <sup>b</sup>	int. <sup>c</sup>	freq. <sup>b</sup>	int. <sup>c</sup>
C-H str	3235.4	(15)	3223.5		2406.6	(13)
W-H str <sup>d</sup>	1970.9	(97)	1970.9		1394.4	(48)
W-H str <sup>d</sup>	1959.4	(245 × 2)	1959.4		1393.0	(126 × 2)
C=W str	1056.9	(19)	1022.4		1005.9	(14)
W-H <sub>2</sub> bend	847.9	(24 × 2)	847.6		609.3	(2 × 2)
W=C-H bend	737.9	(25 × 2)	730.9		578.5	(26 × 2)
sym WH <sub>3</sub> def	676.1	(42)	675.6		482.5	(22)
WH <sub>3</sub> rock	596.6	(64 × 2)	596.6		422.9	(33 × 2)

<sup>a</sup> B3LYP/6-311++G(3df, 3pd)/SDD. <sup>b</sup> Frequencies, cm<sup>-1</sup>. <sup>c</sup> Intensities, km/mol. Double intensities are for *e* modes, others are *a*<sub>1</sub> modes. <sup>d</sup> Strongest modes for CD≡WH<sub>2</sub>D are 1394.4(113), 1958.9(241), and 1967.0(146) and for CH≡WHD<sub>2</sub> are 1394.0(131), 1394.1(75), and 1962.8(193).

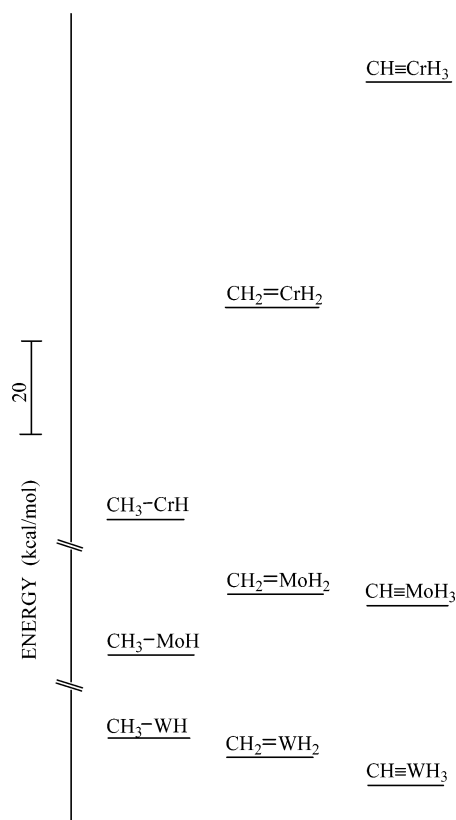
**Table 5.** Calculated Geometrical Parameters, Harmonic Vibrational Frequencies, and Energy Differences for Triplet CH<sub>2</sub>=WH<sub>2</sub> Obtained with Various Theoretical Methods<sup>a</sup>

	MP2	MP4SDQ	CCSD	VSXC
<i>r</i> (C=W)	1.781	1.828	1.874	1.869
<i>r</i> (C-H1)	1.135	1.126	1.118	1.118
<i>r</i> (C-H2)	1.078	1.079	1.080	1.082
<i>r</i> (W-H3)	1.710	1.726	1.734	1.729
<i>r</i> (W-H4)	1.759	1.760	1.757	1.752
< (W-C-H1)	83.1	86.9	91.0	91.2
< (W-C-H2)	158.2	156.0	152.5	152.0
< (C-W-H3)	107.1	109.1	110.2	108.9
< (C-W-H4)	128.8	128.2	127.4	127.3
<i>ν</i> (W-H3)	2009	1963	1929	1901
<i>ν</i> (W-H4)	1915	1902	1887	1846
<i>ν</i> (C=W str)	1015	867	851	858
<i>ν</i> (CH <sub>2</sub> wag)	795	740	677	668
Δ <i>E</i>	14.4	6.1	2.5	5.1

<sup>a</sup> Bond lengths, *r*, in Ångstrom units; bond angles, <, in degrees; vibrational frequencies, *ν*, in cm<sup>-1</sup>; energy difference, Δ*E*, between optimized C<sub>2v</sub> and C<sub>3</sub> geometries, in kJ/mol (see text): SDD+2f/TZ2P basis used (see text).

calculated vibrational frequencies and results from a similar Mo investigation.<sup>14</sup>

**CH<sub>3</sub>-CrH.** The major product absorption at 1623.9 cm<sup>-1</sup> for Cr and CH<sub>4</sub> (Figures 1 and 2) has weaker associated bands at 582.3 and 521.5 cm<sup>-1</sup>. These bands increase together slightly on visible and markedly on near-ultraviolet irradiation. This corresponds to weak 420 nm and very strong 335


**Figure 7.** Relative energies of the lowest electronic states of CH<sub>3</sub>-MH, CH<sub>2</sub>=MH<sub>2</sub>, and CH≡MH<sub>3</sub>. The nearby states of the Mo and W complexes are involved in reversible α-H transfer photochemistry.

nm absorption by Cr atoms in solid argon,<sup>27</sup> which is necessary to activate Cr to react with CH<sub>4</sub>.<sup>28</sup>

The strong 1623.9 cm<sup>-1</sup> absorption shows no <sup>13</sup>C shift, and the deuterium counterpart at 1172.3 cm<sup>-1</sup> defines a 1623.9/1172.3 = 1.385 H/D ratio, which is appropriate for a Cr-H stretching mode. The same two bands are observed with CH<sub>2</sub>D<sub>2</sub>. The strongest such mode for CrH<sub>2</sub> appears at 1614.5 cm<sup>-1</sup> in solid argon,<sup>17</sup> and the analogous mode was observed for CH<sub>3</sub>-MoH at 1728.0 cm<sup>-1</sup>.<sup>14</sup>

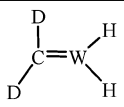
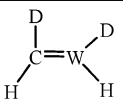
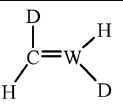
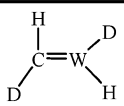
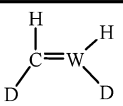
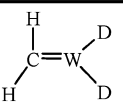
The methylhydride CH<sub>3</sub>-CrH is by far the most stable reaction product (Figure 7). The three strongest observable

(27) Pellin, M. J.; Gruen, D. M.; Fisher, T. Foosnaes, T. *J. Chem. Phys.* **1983**, *79*, 5871.

(28) Bloomberg, M. R. A.; Siegbahn, P. E. M.; Swensson, M. *J. Am. Chem. Soc.* **1992**, *114*, 6095.

(26) Barnes, M.; Gillett, D. A.; Merer, A. J.; Metha, G. F. *J. Chem. Phys.* **1996**, *105*, 6168.

**Table 6.** C–H and W–H Stretching Frequencies ( $\text{cm}^{-1}$ ) Calculated at the CCSD Level for CHD=WHD Mixed-Isotopic Molecules<sup>b</sup>

		
1, 2-D	1, 3-D	1, 4-D
2398.7 (2) <sup>a</sup>	3233.2 (2)	3233.2 (2)
2080.8 (1)	2093.8 (1)	2093.4 (13)
1929.3 (177)	1887.9 (302)	1927.5 (186)
1886.6 (316)	1368.8 (99)	1340.2 (154)
		
2, 3-D	2, 4-D	3, 4-D
2874.1 (3)	2874.0 (4)	3238.0 (1)
2375.7 (3)	2375.7 (3)	2859.2 (5)
1888.6 (300)	1927.5 (185)	1369.4 (49)
1368.8 (99)	1341.7 (154)	1337.1 (125)

<sup>a</sup>Intensities,  $\text{km/mol}$ .<sup>b</sup> (1 is the agostic C–H(D) and 4 is the long W–H(D) trans to the agostic H(D)).

infrared absorptions calculated for  $\text{CH}_3\text{--CrH}$  are at 1674.2, 603.3, and 535.9  $\text{cm}^{-1}$  (Table 2). The latter  $\text{CH}_3$  rocking modes are computed to shift 4.3 and 2.6  $\text{cm}^{-1}$  on  $^{13}\text{C}$  substitution and our bands at 582.3 and 521.5  $\text{cm}^{-1}$  shift 4.4 and 2.5  $\text{cm}^{-1}$ , which is in excellent agreement with the calculations. Therefore, the  $\text{CH}_3\text{--CrH}$  insertion product is identified through the match of three infrared bands and isotopic counterparts to frequencies computed using DFT.

The strongly absorbing Cr–H stretching modes of  $\text{CH}_2=\text{CrH}_2$  were predicted about 100  $\text{cm}^{-1}$  above the strong band for  $\text{CH}_3\text{--CrH}$ , and no such absorptions were observed. This 47 kcal/mol higher energy isomer is apparently not formed in these experiments. We note that very few Cr methyldene complexes are known.<sup>11</sup>

**$\text{CH}_3\text{--WH}$ .** The spectrum of W and  $\text{CH}_4$  reaction products reveals two major groups of product absorptions, which reversibly interconvert upon  $\lambda > 530$  nm and 240–380 nm irradiation sequences. The II set exhibits two strong M–H stretching frequencies, like  $\text{CH}_2=\text{MoH}_2$  and  $\text{CH}_2=\text{ZrH}_2$ ,<sup>5,14</sup> which correlates reasonably well with the computed frequencies for  $\text{CH}_2=\text{WH}_2$  (Table 3). The III set exhibits the highest two W–H frequencies observed here and includes four other modes, which characterize  $\text{CH}\equiv\text{WH}_3$  (Table 4). The strongest infrared absorption of  $\text{CH}_3\text{--WH}$  is computed at 1908  $\text{cm}^{-1}$ , which is the same as the lower W–H stretching mode for  $\text{CH}_2=\text{WH}_2$ . The weaker I band at 1822.2  $\text{cm}^{-1}$  is apparently not a site splitting for the 1817.2  $\text{cm}^{-1}$  II band, as the 1864.5  $\text{cm}^{-1}$  II band lacks such a satellite absorption. Furthermore, the I band increases more on UV irradiation than the II absorptions. This could derive from the rearrangement of III or from the direct excitation of W atoms to react with  $\text{CH}_4$ . The 240–380 nm irradiation covers the  $^5\text{D} \rightarrow ^5\text{F}$  resonance absorption of W on the basis of the matrix absorption spectrum and the gas-phase lines,<sup>29,30</sup> and this excitation can reasonably be expected to activate the W

reaction with  $\text{CH}_4$ . Finally, these bands are in the W–H stretching region, but none of them was produced in previous investigations with  $\text{H}_2$  as the reagent.<sup>25</sup>

The weak but sharp 1822.2  $\text{cm}^{-1}$  absorption shows no  $^{13}\text{C}$  shift, but any D counterpart is masked by  $\text{CH}_4$  impurity absorption (Figure 3). The first  $\text{CH}_3\text{--WH}$  insertion product is the highest energy species formed from W and  $\text{CH}_4$  (Figure 7), and we expect its yield to be low, owing to favorable rearrangement to more stable isomers, in contrast to the Cr case. We tentatively assign the 1822.2  $\text{cm}^{-1}$  absorption to the  $\text{CH}_3\text{--WH}$  insertion product.

**$\text{CH}_2=\text{WH}_2$ .** The two strong, sharp II absorptions at 1817.2 and 1864.5  $\text{cm}^{-1}$  are favored by near-ultraviolet irradiation. These bands exhibit no significant  $^{13}\text{C}$  shift, and their D counterparts are found at 1303.1 and 1336.2  $\text{cm}^{-1}$ . The H/D ratios, 1.384 and 1.395, are appropriate for W–H stretching modes, and the difference is probably due to a small amount of antisymmetric and symmetric character<sup>31</sup> of these two predominantly longer W–H and shorter W–H bond stretching modes.

The CCSD frequency calculation for  $\text{CH}_2=\text{WH}_2$  (Table 3) predicts two strong W–H stretching modes at 1929.3 and 1887.5  $\text{cm}^{-1}$ . These are 3.5% and 3.9% higher than observed, which is reasonable considering anharmonicity and this level of theory.<sup>32,33</sup> Of more importance, the calculated 41.8  $\text{cm}^{-1}$  W–H stretching frequency difference is in large part due to inequivalence in the two W–H bonds arising from agostic distortion, as the calculated bond stretching force constants

(30) Moore, C. E. *Atomic Energy Levels*, Nat. Bur. Stds, Circular 467, Washington, D. C., 1952.

(31) The  $G$  matrix elements for symmetric and antisymmetric modes of a  $\text{MH}_2$  group are different:  $G_{\text{sym}} = \mu\text{H} + \mu\text{M} + \mu\text{M} \cos \alpha$  and  $G_{\text{antisym}} = \mu\text{H} + \mu\text{M} - \mu\text{M} \cos \alpha$  where  $\mu$  is the reduced (i.e., inverse) mass. Thus, for  $90^\circ < \alpha < 180^\circ$ , the sym mode has less metal and hence more H participation.

(32) Scott, A. P.; Radom, L. *J. Phys. Chem.* 1996, 100, 16502.

(33) Comparable CCSD calculations recently performed for  $\text{CH}_2=\text{ZrH}_2$  and  $\text{CH}_2=\text{HfH}_2$  give M–H stretching frequencies 5–7% higher than argon matrix observations.

(29) Schoch, F.; Kay, E. *J. Chem. Phys.* 1973, 59, 718.

differ by 4.2% and the interaction force constant linking them is very small; the band separation observed,  $47.3\text{ cm}^{-1}$ , is close to this calculated value. The B3LYP calculation finds only a  $14\text{ cm}^{-1}$  separation, as the W–H bonds were calculated to be of the same length at this level of theory, which does not fit experiment.

The next observable mode predicted (CCSD) for  $\text{CH}_2\text{=WH}_2$  at  $851.3\text{ cm}^{-1}$  is appropriate in position for the II band at  $847.8\text{ cm}^{-1}$ . The observed band is a mixed mode involving mostly hydrogen on the basis of the isotopic shifts. The next strongest band is the  $\text{CH}_2$  wag computed at  $676.9\text{ cm}^{-1}$  with  $5.1\text{ cm}^{-1}$   $^{13}\text{CH}_2$  and  $151.5\text{ cm}^{-1}$   $\text{CD}_2$  shifts. These are in reasonable agreement with the observed  $651.5\text{ cm}^{-1}$  absorption and  $4.6$  and  $145.3\text{ cm}^{-1}$  isotopic shifts allowing for anharmonicity. The C–H stretching modes are calculated to be too weak to observe at all levels of theory. Furthermore, in one case where C–H stretching modes have been observed ( $2985.8$ ,  $3079.6\text{ cm}^{-1}$ ) for the rather different molecule  $\text{CH}_2\text{=Re(O)}_2\text{OH}$ ,<sup>34</sup> these bands would be masked by our methane precursor.

The strongest experimental evidence for agostic distortion is found in the spectrum for  $\text{CHD=WHD}$  where the W–H and W–D stretching modes should differ slightly from the bands observed with  $\text{CH}_4$  and  $\text{CD}_4$  reactions. We observe weak absorptions at  $1864.8$ ,  $1863.1$ ,  $1820.3$ ,  $1818.2$ , and  $1816.2\text{ cm}^{-1}$  (marked II in Figure 5) and one band at  $1336.9\text{ cm}^{-1}$  (not shown), which display the characteristic species II growth on UV irradiation. These bands can be assigned to mixed  $\text{CHD=WHD}$  isomers with the help of CCSD mixed isotopic frequency calculations (Table 6). The highest and lowest absorptions at  $1864.8$  (shoulder) and  $1816.2\text{ cm}^{-1}$  match calculations for  $\text{CD}_2\text{=WH}_2$  in that the upper W–H stretching mode is unshifted and the lower W–H mode is red-shifted  $0.9\text{ cm}^{-1}$ . One strong new band at  $1863.1\text{ cm}^{-1}$  is a good match for both 1,4-D and 2,4-D  $\text{CHD=WHD}$  isomers (1 is the long agostic C–H(D) bond and 4 is the trans, long W–H(D) bond), as both are computed to red-shift  $1.8\text{ cm}^{-1}$  from  $\text{CH}_2\text{=WH}_2$  and the  $1863.1\text{ cm}^{-1}$  band is down by  $1.4\text{ cm}^{-1}$ . The other strong new band at  $1820.3\text{ cm}^{-1}$  is up  $3.0$  from  $\text{CH}_2\text{=WH}_2$ , and the 2,3-D isomer is computed to be  $2.0\text{ cm}^{-1}$  higher. (The  $1820.3\text{ cm}^{-1}$  band could in principle be due to  $\text{CHD}_2\text{-W-H}$ , but our calculations show a negligible shift from the  $\text{CH}_3\text{-W-H}$  frequency, which rules out this possibility.) A median peak at  $1818.2\text{ cm}^{-1}$  is  $0.9\text{ cm}^{-1}$  higher than  $\text{CH}_2\text{=WH}_2$ , and the 1,3-D isomer is calculated to be  $1.1\text{ cm}^{-1}$  higher. The one new methyldene band in the W–D stretching region at  $1336.9\text{ cm}^{-1}$  (not shown) is  $0.7\text{ cm}^{-1}$  higher than  $\text{CD}_2\text{=WD}_2$ , and the 1,4-D isomer is calculated to be  $0.8\text{ cm}^{-1}$  higher. In summary, we have provided experimental and computational evidence for three of the four mixed asymmetric agostic  $\text{CHD=WHD}$  isomers.

Our calculations using CCSD imposing  $C_{2v}$  symmetry give a  $0.6\text{ kcal/mol}$  higher energy structure, with an imaginary  $i179\text{ cm}^{-1}$   $\text{CH}_2$  rocking mode, and antisymmetric and

symmetric W–H stretching frequencies separated by  $12.0\text{ cm}^{-1}$ . Furthermore, the cis and trans  $\text{CHD=WHD}$  molecules give the same calculated W–H(D) stretching frequencies, which are close to the average of the  $\text{CH}_2\text{=WH}_2$  and  $\text{CD}_2\text{=WD}_2$  values. The observed  $\text{CHD=WHD}$  bands are close to the actual  $\text{CH}_2\text{=WH}_2$  and  $\text{CD}_2\text{=WD}_2$  values, as predicted for the distorted structure (Table 6). The  $\text{CHD=WHD}$  spectra (Figure 5) provide further experimental evidence for a distorted agostic molecule.

The C=W double-bond length of  $1.874\text{ \AA}$  computed here at the CCSD level for the tungsten methyldene dihydride complex,  $\text{CH}_2\text{=WH}_2$ , compares favorably with X-ray measurements in the  $1.88$ ,  $1.943$ ,  $1.975\text{ \AA}$  range for C=W bonds in ligated complexes of the general form  $\text{R}_1\text{R}_2\text{C=WX}_1\text{X}_2$ , which have been reviewed by Schrock.<sup>11</sup>

It is interesting to compare the isotopic frequencies calculated for  $\text{CH}_2\text{=WH}_2$  using B3LYP, which gave a symmetrical structure, with those calculated using the VSXC density functional and CCSD (Tables 3 and S2), which found almost identical distorted agostic structures. First, the diagnostic chromophore is the  $\text{WH}_2$  group stretching modes, and distortion changes these bond lengths relative to each other and the two frequencies observed at  $1817.2$  and  $1864.5\text{ cm}^{-1}$  separated by  $47.3\text{ cm}^{-1}$ . The B3LYP calculation predicts a  $14\text{ cm}^{-1}$  separation, CCSD  $41.8\text{ cm}^{-1}$ , and VSCX  $54.3\text{ cm}^{-1}$ . Mode mixing is expected to differ with the methods, and this is shown in the C-13 shifts for the important mostly C=W stretching and  $\text{CH}_2$  wagging modes (ranging from  $14.3$  to  $19\text{ cm}^{-1}$  for the former to  $5.1$  to  $6.1\text{ cm}^{-1}$  for the latter). It is perhaps reassuring that the  $\text{CH}_2$  wagging mode observed at  $651.5\text{ cm}^{-1}$  with a  $4.6\text{ cm}^{-1}$  C-13 shift is predicted slightly higher ( $698$ ,  $676.9$ ,  $667.7\text{ cm}^{-1}$ ) with all three methods, which is expected for harmonic calculations of anharmonic frequencies at all levels of theory.

The challenge that  $\text{CH}_2\text{=WH}_2$  poses to electronic structure theory is emphasized by the data presented in Table 5. Note first the *tiny* energy differences between the optimized  $C_{2v}$  and  $C_s$  structures (the former being a transition state), despite the large geometrical changes involved (the  $\text{CH}_2$  group pivots by some  $30^\circ$ ). Second, note the large differences between predictions made with the various methods. As the level of theory is improved from MP2 through MP4SDQ to CCSD, the predicted C=W bond length changes by nearly  $0.1\text{ \AA}$ , the extent of the agostic distortion decreases markedly, and consequently, the difference between the two W–H stretching frequencies decreases from  $94$  (MP2) to  $42\text{ cm}^{-1}$  (CCSD). It is striking that the CCSD vibrational results are both reasonably accurate in an absolute sense and more accurate than those obtained with MP2 or MP4SDQ theory for each of the four bands that have been observed for  $\text{CH}_2\text{=WH}_2$ . However, the present CCSD calculations are less than perfect in two respects. First, spin contamination is fairly serious in the underlying UHF wave function, as the value of  $\langle S^2 \rangle$  is  $2.54$ , whereas it should be  $2.00$ . Second, the value of the CCSD T1 diagnostic is  $0.063$ , which is large enough to show that a single-reference method such as CCSD may not be sufficient. We have already noted that the B3LYP version of DFT does not describe the agostic distortion

(34) Morris, L. J.; Downs, A. J.; Greene, T. M.; McGrady, G. S.; Herrmann, W. A.; Sirsch, P.; Scherer, W.; Gropen, O. *Organometallics* **2001**, *20*, 2344.



properly in  $\text{CH}_2=\text{WH}_2$ . However, it is not alone: we have tested 12 different functionals with the bases described above, and only one of them, VSXC,<sup>18e</sup> gave satisfactory results as judged by the predicted vibrational spectra. As shown in Tables 5 and S2, the structural and vibrational results obtained with the VSXC version of DFT are very close to those obtained with CCSD theory. Given the much smaller computational demands of VSXC theory than CCSD for molecules that contain more than a handful of atoms, it will be of considerable importance to discover whether VSXC is consistently successful in applications concerning vibrational spectroscopy.

**$\text{CH}\equiv\text{WH}_3$ .** The III absorption group is enhanced on  $\lambda > 530$  nm irradiation. Our B3LYP calculation shows that  $\text{CH}\equiv\text{WH}_3$  is a stable trigonal molecule. The strongest infrared absorption is predicted to be the doubly degenerate W–H stretching mode at  $1959.4\text{ cm}^{-1}$  with a weaker symmetric W–H stretching mode at  $1970.9\text{ cm}^{-1}$ . The strong  $1896.3\text{ cm}^{-1}$  and weaker  $1907.5\text{ cm}^{-1}$  III absorptions are assigned accordingly. Note the agreement between the calculated  $11.5\text{ cm}^{-1}$  and observed  $11.2\text{ cm}^{-1}$  mode separation! These bands show no  $^{13}\text{C}$  shift, and the stronger one shifts to  $1362.8\text{ cm}^{-1}$  with  $\text{CD}_4$  (1.391 ratio). The scale factors (observed/calculated) for the three tungsten–hydride species observed here, namely 0.968, 0.968 ( $\text{CH}\equiv\text{WH}_3$ ), 0.952, 0.970 ( $\text{CH}_2=\text{WH}_2$ ), and 0.955 ( $\text{CH}_3-\text{WH}$ ), are compatible with scale factors for other compounds.<sup>32</sup> This agreement supports our assignments.

With  $\text{CH}_2\text{D}_2$ , we expect to form  $\text{CD}\equiv\text{WH}_2\text{D}$  and  $\text{CH}\equiv\text{WHD}_2$ , and these should in principle give additional mixed H,D isotopic bands for the strong W–H stretching modes. Unfortunately, the W–D stretching modes are not separated enough to resolve, but our calculations predict two W–H stretching modes for  $\text{CD}\equiv\text{WH}_2\text{D}$  that are 0.5 below and  $7.6\text{ cm}^{-1}$  above the strong  $\text{CH}\equiv\text{WH}_3$  band. The observed stronger  $1895.6$  and weaker  $1903.4\text{ cm}^{-1}$  bands (upper short arrow, Figure 4d) are 0.7 below and  $7.1\text{ cm}^{-1}$  above the strong  $1896.3\text{ cm}^{-1}$  band, which is excellent agreement. For  $\text{CH}\equiv\text{WHD}_2$ , we predict the W–H stretching mode  $3.4\text{ cm}^{-1}$  above the strong  $\text{CH}\equiv\text{WH}_3$  band and the new  $1899.3\text{ cm}^{-1}$  band (lower short arrow) is  $3.0\text{ cm}^{-1}$  higher. The above isotopic data substantiate the characterization of a trigonal  $\text{WH}_3$  group with two W–H stretching vibrational modes, one degenerate and one nondegenerate.

The next important mode predicted for  $\text{CH}\equiv\text{WH}_3$  is the  $\text{C}\equiv\text{W}$  stretching mode at  $1056.9\text{ cm}^{-1}$ . This mode is observed as a site split band at  $1008.9$ ,  $1003.4$ , and  $995.1\text{ cm}^{-1}$ , much as the upper mode is site split at  $1896.3$ ,  $1893.1$ , and  $1888.3\text{ cm}^{-1}$ . The  $^{13}\text{C}$  shift predicted by DFT for this band is  $34.5\text{ cm}^{-1}$  and our  $1003.4\text{ cm}^{-1}$  band shifts  $32.7\text{ cm}^{-1}$ , and the computed D shift is  $51.0\text{ cm}^{-1}$  and our band shifts  $50.1\text{ cm}^{-1}$ . This excellent agreement in mode position and isotopic shifts confirms the observation of the diagnostic  $\text{C}\equiv\text{W}$  stretching mode. This mode has been observed at  $1006\text{ cm}^{-1}$  for  $\text{H}-\text{C}\equiv\text{W}$ ,<sup>25</sup> and our DFT calculation predicts  $1057.4\text{ cm}^{-1}$ , which supports our assignment for  $\text{CH}\equiv\text{WH}_3$ .

Two weaker absorptions at  $726.7$  and  $658.0\text{ cm}^{-1}$  exhibit the group III photochemistry, and these frequencies are

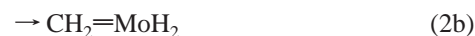
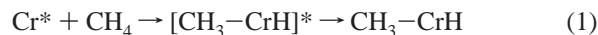
appropriate for computed  $737.9\text{ cm}^{-1}$  antisymmetric mostly  $\text{H}-\text{C}\equiv\text{W}$  bending and  $676.1\text{ cm}^{-1}$  symmetric  $\text{WH}_3$  deformation modes. Unfortunately no isotopic data were found for these weaker bands, but the former is in good agreement with the bending mode observed at  $660\text{ cm}^{-1}$  for  $\text{H}-\text{C}\equiv\text{W}$ .<sup>26</sup> The final  $\text{WH}_3$  rocking mode is predicted at  $596.6\text{ cm}^{-1}$ , and this band is observed here at  $579.4\text{ cm}^{-1}$  without any  $^{13}\text{C}$  shift.

In summary, we have definitively identified the trigonal  $\text{CH}\equiv\text{WH}_3$  molecule from the matrix infrared spectrum through the observation of two stretching modes for the  $-\text{WH}_3$  group, appropriate W–H stretching modes for the mixed  $-\text{WH}_2\text{D}$  and  $-\text{WHD}_2$  species, and the match with isotopic frequency predictions from DFT calculations. The  $\text{HC}\equiv\text{W}$  stretching mode is characterized by  $^{13}\text{C}$  and D shifts. Three modes involving  $\text{HC}\equiv\text{W}$  bending,  $\text{WH}_3$  deformation, and rocking also correlate well with frequencies predicted by DFT. The matrix infrared spectrum thoroughly characterizes this novel molecule from a vibrational perspective.

The  $\text{C}\equiv\text{W}$  triple-bond length we have computed here at the DFT level for the new  $\text{CH}\equiv\text{WH}_3$  molecule,  $1.742\text{ \AA}$ , compares favorably with that measured for  $\text{H}-\text{C}\equiv\text{W}$  in the gas phase,<sup>26</sup>  $1.732\text{ \AA}$ , and with X-ray values in the  $1.745\text{--}1.75\text{ \AA}$  range for ligated  $\text{RC}\equiv\text{WX}_1\text{X}_2\text{X}_3$  complexes.<sup>11</sup> Furthermore, our computed  $\text{C}\equiv\text{W}$  triple-bond length is shorter than the  $1.80\text{ \AA}$  value computed for the isoelectronic  $\text{CH}\equiv\text{TaH}_3^-$  anion at the MC/LMO/CI level of theory.<sup>35</sup> We note that this multiconfiguration calculation gives a  $C_{3v}$  structure with a triple metal–carbon ( $\sigma_{\text{MC}}(2)$ ,  $\pi_{\text{MC}}(1)^2$ ,  $\pi_{\text{MC}}(2)^2$ ) bond.

The antisymmetric W–H stretching frequency for  $\text{CH}\equiv\text{WH}_3$  ( $1896.3\text{ cm}^{-1}$ ) is higher than the analogous mode for  $\text{CH}\equiv\text{MoH}_3$  ( $1830.0\text{ cm}^{-1}$ ).<sup>14</sup> This relationship is found for the binary hydrides.<sup>36</sup> On the other hand, the  $\text{W}\equiv\text{C}-\text{H}$  bending mode ( $726.7\text{ cm}^{-1}$ ) is lower than the  $\text{Mo}\equiv\text{C}-\text{H}$  bending mode ( $751.2\text{ cm}^{-1}$ ) in the corresponding molybdenum compound.

**Reaction Mechanisms.** Laser-ablated Cr, Mo, and W atoms are sufficiently energetic to overcome the activation energy for C–H insertion<sup>28</sup> to form  $\text{CH}_3-\text{CrH}$ ,  $\text{CH}_3-\text{MoH}$ , and  $\text{CH}_3-\text{WH}$ , reactions 1, 2a, and 3a, respectively.



The activated  $[\text{CH}_3-\text{MH}]^*$  thus formed can be relaxed by the condensing matrix, and the methyl metal hydrides are trapped. In the Cr case, the methyldiene and methyldiyne

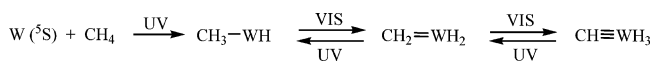
(35) Cundari, T. R.; Gordon, M. S. *J. Am. Chem. Soc.* **1992**, *114*, 539.

(36) Andrews, L. *Chem. Soc. Rev.* **2004**, *33*, 123.

isomers are so much higher in energy (Figure 7) that only the insertion product  $\text{CH}_3\text{-CrH}$  is formed (I in Figures 1 and 2). However, for Mo and W, the methylenide and methylidyne isomers are close in energy (12 and 11 kcal/mol for Mo, and  $-1$  and  $-11$  kcal/mol for W) and facile  $\alpha\text{-H}$  transfers occur to give these products, reactions 2b, 2c, 3b, and 3c. The increasing stability of higher hydrides with tungsten is due in part to increasing strength of the metal–hydride bond upon going down the family group,<sup>37</sup> and this is displayed by our gross reaction product spectra (Figure 2). A similar relationship has been found for the analogous fluorine-substituted derivatives prepared from Group 6 metal atoms and methyl fluoride.<sup>15</sup> Finally, we must point out that an early investigation of methane activation by photoexcited metal atoms in pure solid methane failed to yield an insertion product for chromium.<sup>38</sup> However, the  $\text{CH}_3\text{-CrH}$  product formed here on laser ablation and isolated in excess solid argon increased substantially on  $>290$  nm irradiation.

Subsequent visible ( $\lambda > 530$  nm) and near-ultraviolet (240–380 nm) irradiations initiate electronic excitations, which foster successive  $\alpha\text{-H}$  transfers<sup>39</sup> among the three  $\text{CH}_3\text{-WH}$ ,  $\text{CH}_2\text{=WH}_2$ , and  $\text{CH}\equiv\text{WH}_3$  molecules. Note from the infrared spectra in Figure 2 that visible light rearranges all I and II to III and that subsequent near-ultraviolet irradiation restores I and II at the expense of III, although III is the lowest-energy isomer. We suggest that competing rate processes are important here, as the excited triplet  $\text{CH}_2\text{=WH}_2$  state must relax in the matrix faster than  $\alpha\text{-H}$  back transfer to form  $\text{CH}_3\text{-WH}$ . These processes are completely reversible without side reactions. Hence, we have a dynamic

#### Scheme 1



photochemical  $\alpha\text{-H}$  transfer equilibrium established among the  $\text{CH}_3\text{-WH}$ ,  $\text{CH}_2\text{=WH}_2$ , and  $\text{CH}\equiv\text{WH}_3$  species, Scheme 1, in the excited states reached by visible and near-ultraviolet irradiation.

#### Conclusions

Laser-ablated Cr atoms react with  $\text{CH}_4$  in excess argon to give only  $\text{CH}_3\text{-CrH}$ , while W atoms react with  $\text{CH}_4$  to form the  $\text{CH}_3\text{-WH}$ ,  $\text{CH}_2\text{=WH}_2$ , and  $\text{CH}\equiv\text{WH}_3$  molecules with increasing yield in this order of product stability. These molecules are identified from infrared spectra by isotopic substitution and DFT/CCSD frequency calculations. Simple tungsten methylenide and methylidyne hydride molecules are reversibly interconverted by  $\alpha\text{-H}$  transfers upon visible and ultraviolet irradiations. Matrix infrared spectra and DFT calculations show that  $\text{CH}\equiv\text{WH}_3$  is a stable molecule with  $C_{3v}$  symmetry. Although B3LYP calculations with the large Gaussian<sup>18</sup> basis set 6-311++G(3df,3pd) and SDD pseudo-potential provide excellent agreement with the observed spectrum of singlet  $\text{CH}\equiv\text{WH}_3$ , the agreement found for triplet  $\text{CH}_2\text{=WH}_2$  is not as good, and CCSD calculations were required to show agostic distortion in the  $\text{CH}_2\text{=WH}_2$  methylenide and the proper  $\text{WH}_2$  stretching frequency separation.

**Acknowledgment.** We appreciate support from NSF Grant No. CHE 03-52487 to L.A.

**Supporting Information Available:** Tables S1 and S2. This material is available free of charge via the Internet at <http://pubs.acs.org>.

IC051090H

(37) Tilset, M.; Parker, V. D. *J. Am. Chem. Soc.* **1989**, *111*, 6711.

(38) Billups, W. E.; Konarski, M. M.; Hauge, R. H.; Margrave, J. L. *J. Am. Chem. Soc.* **1980**, *102*, 7394.

(39) Crabtree, R. H. *The Organometallic Chemistry of the Transition Metals*; Wiley and Sons: New York, 2001; p 190.